A Physical Optics Simulator for Multireflector THz Imaging Systems

Lorena Perez-Eijo, Borja Gonzalez-Valdes, Marcos Arias, Dario Tilves, Yolanda Rodriguez-Vaqueiro, Oscar Rubiños-Lopez, Antonio Pino, *Senior member, IEEE*, Federico García-Rial, *Student Member, IEEE,* Jesús Grajal *Member, IEEE,*

***Abstract*—This work presents a Physical Optics-based simulator for the analysis of THz imaging systems. The simulation starts by calculating the electromagnetic interactions inside the multireflector system and the incident field that the focusing system creates on the target under inspection. In a second step, the electric field that the modeled target scatters back to the system receiver, is also calculated. This allows to predict the imaging behavior of the system for different targets before manufacturing. The simulator results are validated by using measurements from an existing 300 GHz standoff imaging system. This contribution aims to help in the development of better imaging systems for security applications in the near future.**

***Index Terms*—Reflector antennas, submillimeter wavelength imaging, inverse scattering, radar imaging, physical optics.**

I. Introduction

In recent years interest in personal security applications has markedly grown. In this context, active millimeter wave radar has been proved to provide excellent capabilities for the detection and imaging of concealed threat or contraband at security checkpoints [1]–[3]. In particular, the use of active submillimeter (THz) imaging systems is of great interest for the challenging problem of standoff observation. Different systems to achieve through-clothing imaging at standoff ranges of tenths of meters have been presented [4]–[7]. These systems are capable of penetrating opaque materials, preserve the privacy of the explored target and achieve a good image resolution. The area of interest is scanned in a pixel by pixel imaging strategy by using multireflector systems and mechanical fast beam scanning [8]. The theoretical and simulated focusing properties of these kind of systems have been profusely studied in the literature [9], [10]. However, these studies are mainly limited to the properties of the system in transmission, while the response of the imaging to different targets has been mostly based on small sets of measurements.

However, the development of better and more complex THz systems for security applications demands the use of reliable and efficient simulation tools to improve the design and optimization of novel radar configurations before manufacturing. Also, these simulators are of great interest to obtain datasets of realistic examples for automatic target recognition and allow for the use of model-based inversion algorithms [11] to improve the detection and identification abilities.

In [12] a thorough review of the available simulators for these kind of THz systems is presented. It concludes that most of the simulators for concealed object detection are based on ray-tracing and corrected using different scattering models as Kirchoff [13] or bidirectional reflectance distribution function (BRDF) [14].

In this work a Physical Optics (PO) based simulator for THz imaging systems is presented. PO [15], [16] is a well-known asymptotic high frequency computational technique traditionally used to analyze the behavior of reflector antennas in terms of gain, secondary lobe level or cross-polar radiation. However, the use of PO to analyze imaging systems at THz frequencies is very challenging due to the large electrical size of the reflector surfaces and the repeated number of simulations that are needed to simulate the pixel-by-pixel operation at multiple frequencies. We have developed an in-house simulator to overcome these limitations. In the simulator PO is used not only to predict the incident field that the focusing system creates on the target under inspection, but also to calculate the electric field that the target scatters back to the receiver through the reflector system. It could be integrated in an optimization framework to design imaging systems according the required specifications in terms of obtained field of view, resolution, dynamic margin, etc. The aforementioned optimization concept refers to design parameters, such as the geometry of each of the elements of the system. In this work, the simulation results are compared with measurements made by a system that already exists, in order to verify the robustness of the simulator. We believe the simulator is specially useful to verify the behavior of the system in terms of resolution, Field of View and other important parameters before fabrication, and also to detect possible problems once the system is manufactured. To our knowledge, these features are not available in a straightforward manner in current commercial simulation software, which is mainly devoted to the design and simulation of antennas in terms of their main transmission parameters.

Manuscript received April, 2019. This work is partially supported by the Spanish National Research and Development Program project TEC2015-65353-R, TEC2015-73908-JIN and TEC2017-87061-C3-1-R, by the European Regional Development Fund (ERDF), and by the Galician Regional Government under project GRC2015/018 and under agreement for funding AtlantTIC (Atlantic Research Center for Information and Communication Technologies.).

The authors would like to thank Mrs. Raquel Miguez-Vazquez and Mr. Adolfo Rodriguez-Uruburo for the English proofreading and their contributions for the article improvement.

Lorena Perez-Eijo, Borja Gonzalez-Valdes, Marcos Arias, Dario Tilves, Yolanda Rodriguez-Vaqueiro, Oscar Rubiños-Lopez and Antonio Pino are with the Atlantic Research Center, Universidad de Vigo, Vigo, Spain. (e-mail: lorena@com.uvigo.es)

Federico García-Rial, Jesús Grajal are with the Information Processing and Telecommunication Center, Universidad Politécnica de Madrid, UPM, Madrid, Spain.

The main contributions of this work are:

i) a PO-based simulator for THz imagers in both transmission and reception, including nearfield interactions between the reflector system and the target under test;

ii) qualitative and quantitative comparisons between simulated and measured results.

The structure of the paper is as follows. The imaging system that is simulated and used to validate the obtained solutions is described in Section II. The details of the implemented PO approach are presented in Section III. The simulation process is described in Section IV. The obtained results are shown in Section V and finally conclusions are provided in Section VI.

II. Simulated 300 GHz imager

The imaging system used to validate the proposed PO approach is based on a Bifocal Elliptical Gregorian Reflector System (BEGRS). The system is capable of generating high resolution images in real time at a standoff distance of 8 m and with a field of view (FoV) of 90 cm $\times$ 50 cm, focusing a 300 GHz beam [17]. A 27 GHz bandwidth is used in the system to ensure good range resolution.

The baseline design consists of two opposite-faced reflector antennas with a common focus. This configuration is similar to the offset confocal elliptical reflector (CEGRS) [9], but their surfaces are shaped to have a better scan capability. Fig. 1 shows the multireflector system configuration.

Fig. 1. Multireflector-based imaging system at 300 GHz used to validate the proposed PO simulator.

The principal elements of this configuration are [12]:

(a) A main reflector aperture which focuses the 300 GHz beam to the target plane.
(b) A parabolic subreflector that radiates the field from the mirror to the main reflector.
(c) A rotating flat mirror placed between the feed reflector and the subreflector which is used to achieve mechanical beam scanning in both elevation and azimuth.
(d) An auxiliar parabolic feed reflector to achieve the collimated beam to feed the subreflector.
(e) A beamsplitter to separate the transmission (Tx) and reception (Rx) paths.

With the BEGRS it is possible to focus a 300 GHz beam at a standoff distance of 8 meters with a cross-range resolution $\Delta CR = 1.6$ cm and a range resolution $\Delta R = 1$ cm. The system operates as a monostatic active radar and the target is placed facing the main reflector at the standoff distance. The auxiliar parabolic reflector is fed by a horn antenna placed at its focus. The proposed simulator uses PO to calculate the incident field created by the feed (modeled as a cos-q) and the nearfield interactions between the reflector surfaces in both transmission (from transmitter to reflectors to target) and reception (from target to reflectors to receiver). The beam splitter effects are not considered in the simulation at this moment and both transmitter and receiver are simulated as placed at the same position

III. Physical Optics Approach

The developed code is based on the computation of the induced currents between two reflecting surfaces. First, the surfaces are imported as CAD models into the program and modeled as a set of triangular patches (see Fig. 2) with three points $\vec{R}_{m_1}$, $\vec{R}_{m_2}$ and $\vec{R}_{m_3}$, that define a central point $\vec{R}_m = \frac{\vec{R}_{m_1}+\vec{R}_{m_2}+\vec{R}_{m_3}}{3}$ and two edge vectors $\vec{v}_{m_{12}} = \vec{R}_{m_2} - \vec{R}_{m_1}$ and $\vec{v}_{m_{13}} = \vec{R}_{m_3} - \vec{R}_{m_1}$. From these vectors, the normal is calculated as $\hat{n}_m = \frac{\vec{v}_{m_{12}} \times \vec{v}_{m_{13}}}{\|\vec{v}_{m_{12}} \times \vec{v}_{m_{13}}\|}$ and the area as $A_m = \frac{\|\vec{v}_{m_{12}} \times \vec{v}_{m_{13}}\|}{2}$.

The process starts by calculating the incident magnetic field $\vec{H}_m$, the incident electric field $\vec{E}_m$ and the incident Poynting vector $\hat{p}_{i_m}$ on the first reflector surface created by a feed modeled as a cos-q. The value of the parameter q is adjusted as a function of the actual horn antenna used to feed the reflector system. Once these three vectors are calculated, the induced currents in the next reflector surface are calculated as follows.

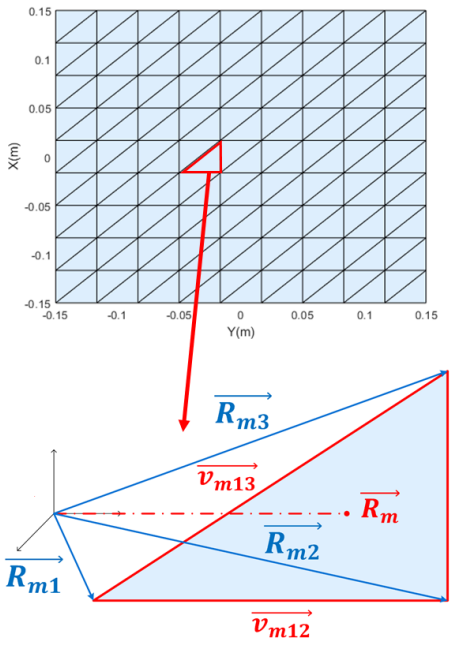

Fig. 2. Triangular mesh and vector notation used in the implementation of the PO simulation.

First, the electric current $\vec{J}_m$ is calculated using the incident magnetic field at the center of each triangle:

$$\vec{J}_m = 2\hat{n}_m \times \vec{H}_m \tag{1}$$

PO nearfield equations are used to calculate magnetic and electric field $\vec{H}_n$, $\vec{E}_n$ at a point $\vec{R}_n$ on the next reflector surface. The position vector between the triangles in both surfaces is $\vec{R}_{mn} = \vec{R}_n - \vec{R}_m$, the distance $R_{mn} = \|\vec{R}_{mn}\|$ and the direction $\hat{R}_{mn} = \frac{\vec{R}_{mn}}{R_{mn}}$.

$$\vec{H}_n = \sum_m \vec{H}_{mn} \tag{2}$$

$$\vec{H}_{mn} = \frac{e^{-jkR_{mn}}}{4\pi R_{mn}^3}\left(1 + jkR_{mn}\right)\left(\vec{J}_m \times \vec{R}_{mn}\right) I_{mn} \tag{3}$$

$$I_{mn} = 2A_m e^{-j\frac{\alpha_{mn}+\beta_{mn}}{3}}\left[\gamma_{mn}\right] \tag{4}$$

where

$$\gamma_{mn} = \left[\frac{\alpha_{mn}e^{j\beta_{mn}} - \beta_{mn}e^{j\alpha_{mn}} + \beta_{mn} - \alpha_{mn}}{\left(\alpha_{mn} - \beta_{mn}\right)\alpha_{mn}\beta_{mn}}\right] \tag{5}$$

$$\alpha_{mn} = k\vec{v}_{m_{12}} \cdot \left(\hat{R}_{mn} - \hat{p}_{i_m}\right) \tag{6}$$

$$\beta_{mn} = k\vec{v}_{m_{13}} \cdot \left(\hat{R}_{mn} - \hat{p}_{i_m}\right) \tag{7}$$

This process is repeated for all the couples of triangles in both reflector surfaces. To obtain the Poynting vector $\hat{p}_{i_n} = Re\{\frac{\vec{E}_n \times \vec{H}_n^*}{\|\vec{E}_n \times \vec{H}_n^*\|}\}$ it is necessary to calculate also the electric field:

$$\vec{E}_n = \sum_m \vec{E}_{mn} \tag{8}$$

$$\vec{E}_{mn} = -\frac{j\eta e^{-jkR_{mn}}}{4\pi k R_{mn}^3}\left[\vec{J}_m\left(-1 - jkR_{mn} + (kR_{mn})^2\right) + \right.$$

$$\left. + \hat{R}_{mn}\left(3 + 3jkR_{mn} - (kR_{mn})^2\right)\left(\hat{R}_{mn} \cdot \vec{J}_m\right)\right] I_{mn} \tag{9}$$

If the distance between both surfaces are much greater than the wavelength, equations (3) and (9) can be simplified as

$$\vec{H}_{mn} = \frac{j}{2\lambda}\frac{e^{-jkR_{mn}}}{R_{mn}}\left(\vec{J}_m \times \hat{R}_{mn}\right) I_{mn} \tag{10}$$

$$\vec{E}_{mn} = \eta\vec{H}_{mn} \times \hat{R}_{mn} \tag{11}$$

This process is sequentially followed for all the reflector surfaces until the induced electric currents on the main reflector are obtained. Next section describes how the interaction with the target under test is obtained.

IV. Simulation Method

A. Simulation process

As stated before, the imaging system is based on a pixel-by-pixel scanning of the target area placed at a prescribed distance from the antenna. Such scanning is obtained by the rotation and tilting of a flat mirror. In the simulation, a rectangular grid in the target area is defined and, by using a polynomial approximation, each pixel position is mapped to the corresponding rotation and tilting angles of the mirror [8]. For each position of the mirror the induced currents on its surface are calculated according to the equations in previous section. The process is repeated until the electric currents on the main surface for steering the beam at each particular position on the target plane are calculated ($\vec{J}_2$ in Fig. 3). To complete the simulation of the system in transmission mode, the incident field on the target under test, modeled as a triangular mesh, is computed by using again the same equations described in Section III.

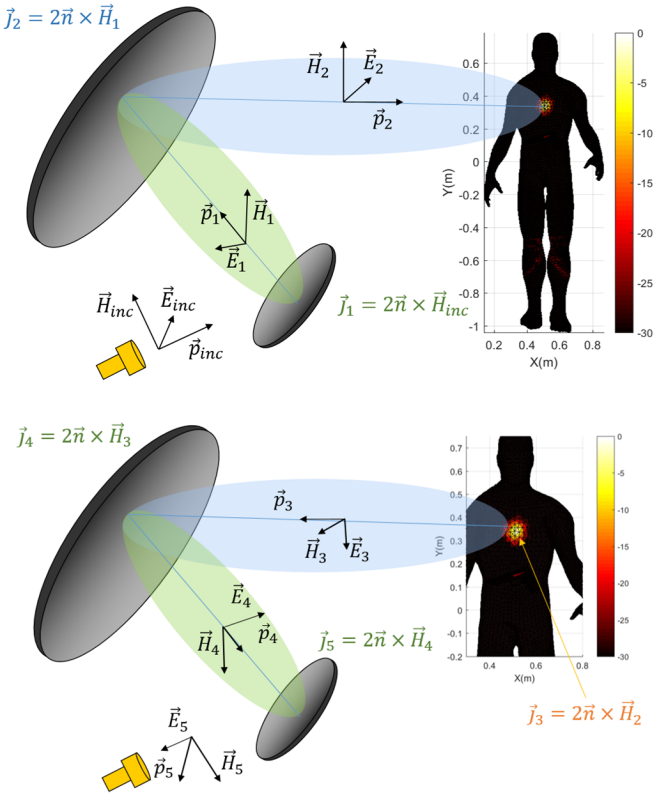

Fig. 3. Description of the PO-based simulation process in transmission (top) and reception (bottom).

The simulation of the imaging system response for the modeled target starts by calculating the induced electric currents on the target, $\vec{J}_3$, from the induced magnetic field $\vec{H}_2$. This part of the process models the different response to the imaging system of different areas of the target depending on their shape, which is a critical factor in these kind of systems [12]. The calculated currents are used to radiate back to the main reflector surface where a new set of currents $\vec{J}_4$ are induced. These currents are used to sequentially radiate to the next reflector surfaces until the electric field at the receiving point

(the focal point of the auxiliar reflector) is calculated according to Section III.

This process is independently repeated for multiple equally spaced frequencies in the radar bandwidth according the desired non-ambiguous range. The simulation process ends when all the pixels on the target plane have been scanned. The output of the program is a matrix with as many rows as pixels and as many columns as frequencies.

B. Simulation optimization

For a large number of pixels and frequencies, the simulation process described above can take a substantial amount of time. Two different approaches have been used to reduce the computational time of the simulator. First, if the triangles of the simulated surfaces are small in terms of wavelength Equation (4) can be simplified as [18]–[20].

$$I_m \approx A_m \quad , \quad \forall n \tag{12}$$

This approximation is used in the radiation between the main reflector and the target being simulated, and it reduces the total computation time about one third.

Second, for further time reduction, the PO codes have been implemented using a GPU through the set of libraries provided by Matlab. Efficient implementation of the code in GPU requires to create two intermediate matrices in order to reduce the number of calculations:

$$c_{mn} = \frac{I_{mn} e^{-jkR_{mn}}}{R_{mn}} \tag{13}$$

with I_{mn} obtained from expression (4) or (12), and

$$\vec{a}_{mn} = c_{mn} \vec{J}_m \times \hat{R}_{mn} \tag{14}$$

$$\vec{H}_n = \frac{j}{2\lambda} \sum_m \vec{a}_{mn} \tag{15}$$

$$\vec{E}_n = \frac{j\eta}{2\lambda} \sum_m \vec{a}_{mn} \times \hat{R}_{mn} \tag{16}$$

The GPU is used through the matlab arrayfun tool, even knowing that full performance is not obtained. The use of CUDA in this application is not possible due to the size of the matrices that must have all the same size. On the other hand, in Matlab is possible to mix vectors with matrices, using significantly less memory than using CUDA.

The computation time of each pixel at a single frecuency is 3 seconds.

C. Signal processing for imaging

As explained in Section I, the imaging system uses a pixel-by-pixel observation strategy. For each observation pixel, the system captures the received field for all studied frequencies, what is defined as burst. Each of the burst is stored in a received data matrix whose rows correspond to the number of bursts and the columns with the number of used frequencies. By applying the Inverse Fast Fourier Transform (IFFT) to each burst, High Resolution Synthetic Range profiles (HRR) are achieved, building a high resolution profile matrix whose columns correspond to the range cells [21].

Range images are created by locating the position of the maximum value of each HRR and the reflectivity ones are achieved by using that maximum HRR value, as shown in Fig. 4. For its representation, the reflectivity image is normalized by its maximum value.

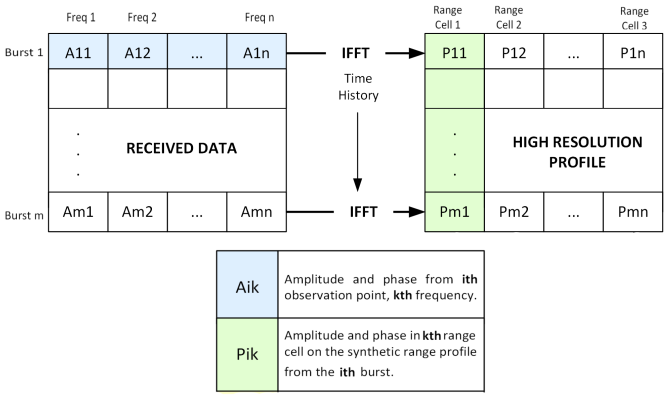

Fig. 4. Description of the imaging algorithm applied to the simulation results.

V. Validation and Results

In this Section, to validate the performance of the presented simulator, the simulation results are compared to measurements obtained using the imaging system described in Section II. Two different targets placed at a standoff distance of 8 m have been considered. The first case is a metallic flat plate which serves as a canonical example to study the response of the imaging system to tilted surfaces. In the second example a female mannequin torso is used to evaluate the range and shape accuracy obtained by using the simulation results. A bandwidth of 27 GHz and an observation pixel size of 1.5 cm have been used. Additive Gaussian noise 40 dB below the maximum signal level has been added to the obtained simulation results before creating the images. Imaging is based on applying an IFFT to the obtained frequency response at each pixel.

The simulations have been performed using the hardware described below:

- 2 × Intel® Xeon® E5-2690 v2 @3GHz processors.
  - RAM: 512 GB
  - Number of Cores: 10 (2 logical cores per physical)
- 1 × NVIDIA GeForce GTX TITAN X
  - Memory: 12 GB (GDDR5 SDRAM)
  - Number of CUDA Cores: 3072

A. Example 1: metallic flat plate

One of the main purposes of the presented simulator is to study the effect of the target shape on the obtained images. Since, at these frequencies, the target response is mainly given

by the specular reflection of the incident beam, these type of configurations can misrepresent certain areas of the target if the response of these areas is below floor noise. This first experiment aims to study this effect.

The measured object is a 47 cm $\times$ 18 cm flat metal plate placed in front of the imaging system. The plate is first measured with its normal pointing to the center of the main reflector, which corresponds to the specular reflection direction. Then, it is rotated around the vertical axis in increments of 1 degree.

For the simulation, a CAD model of the plate is used. An observation grid of 47 cm $\times$ 18 cm in the target area is defined and discretized every 1.5 cm. The imaging system is synthetically pointed to each pixel as described in Section IV-A. Fig. 5 shows the measured and simulated results for different tilt angles. In these plots, the maximum amplitudes of the IFFT of the measured and simulated signal for each pixel are represented. As the plate rotates, the amount of received power decreases rapidly, due to the fact that the antenna is no longer fully capturing the specular reflection from the plate. By comparing the results of the measurements and the simulations a high concordance can be verified.

- Figs. 5(a) and 5(b) show a great fit. In the simulated image it can be seen that the similarity in the central part of the plate is very high, but closer to the corners, the power level received in measurements is slightly lower. These looseness arise due to inaccuracies of position (in practice the target position adjustment at the standoff distance is a really complex task).
- Figs. 5(c), 5(d), 5(e) and 5(f), as in the previous case, show a great fit but although the adjustment is very high in the area of the maximum, due to small inaccuracies in the real position of the target, when moving axially the power drop is slightly higher in the measurements compared to the simulations.
- In Figs. 5(g) and 5(h) apart from observing a good fit between both responses, an edge effect in simulation can be appreciated. This effect is due to the inacuracy of PO simulations when there is an edge highly iluminated.

Fig. 6 shows the difference between the images recovered by measurement and those recovered by simulation. The difference between the two images is calculated by subtracting the simulated image and the measured image (both normalized by their maximum). In certain areas of the recovered images there are higher error values (over 12 dBs). In the lower left corner of the Figs. 6(a) and 6(c) the high error value observed is due to mismatches in the positioning of the OUT. On the left side of the Fig. 6(b) and on the right side of the Fig. 6(d), high error values are also observed, as already explained above, this effect occurs due to the inacuracy of PO simulations when there is an edge highly iluminated.

To quantify the correlation between the simulations and the measurements, the mean-squared error (MSE) for each of the studied metal plate positions, was calculated. Table I shows the obtained results using the following expression:

$$MSE = \frac{1}{n}\sum_{i=1}^{n}(i_{sim} - i_{meas})^2 \tag{17}$$

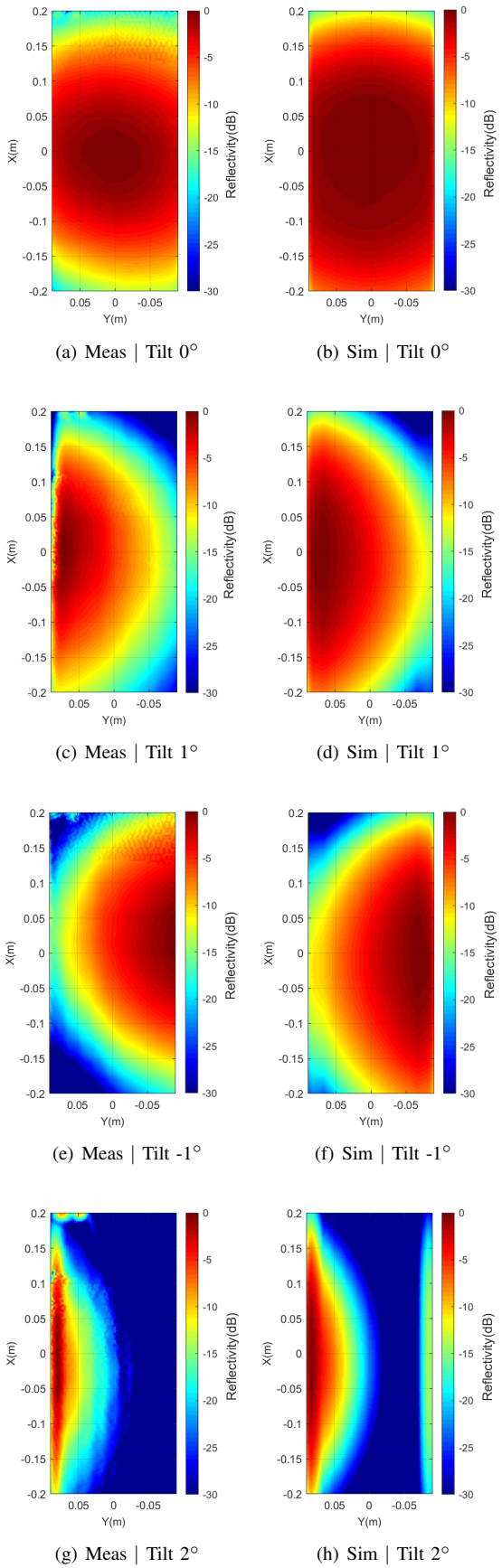

(a) Meas | Tilt 0° (b) Sim | Tilt 0°

(c) Meas | Tilt 1° (d) Sim | Tilt 1°

(e) Meas | Tilt -1° (f) Sim | Tilt -1°

(g) Meas | Tilt 2° (h) Sim | Tilt 2°

Fig. 5. Measured (Meas) VS Simulation (Sim) reconstructed images. Reflectivity in dB relative to the maximum of each image for different tilt angles of the metallic plate is depicted.

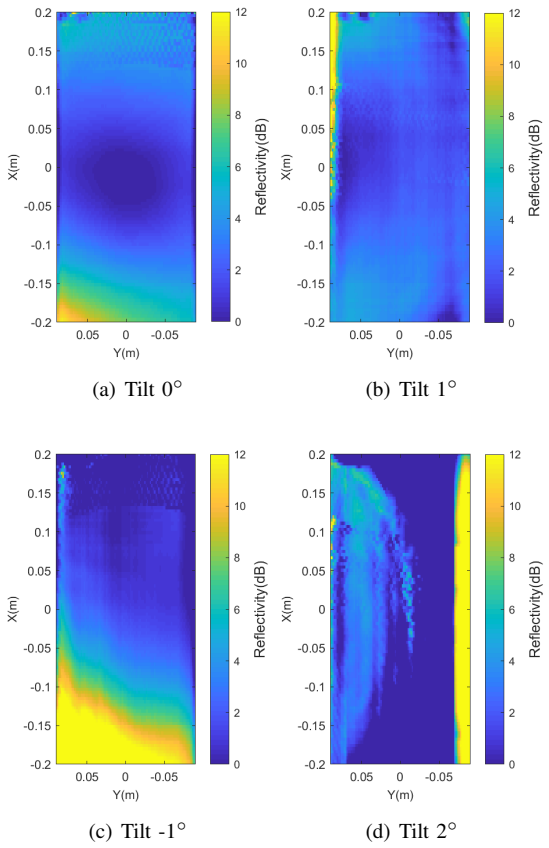

(a) Tilt 0° (b) Tilt 1°

(c) Tilt -1° (d) Tilt 2°

Fig. 6. Subtraction between simulation and measurement recovered images for the different analized tilt angles.

being n the number of elements of each of the images, i_{sim} the elements of the simulation recovered image and i_{meas} the elements of the measured recovered image. For the MSE calculation, the value of each pixel of the images are expressed in natural units.

Tilt (°)	**MSE** (dB)
0	-27.79
1	-34.39
-1	-31.03
2	-43.36

TABLE I
MSE VALUE IN DB FOR EACH OF THE TILTED PLATE CASES UNDER STUDY.

To further explore this specular reflection behavior, the measured and simulated received power at the imaging system receiver as a function of the angle is depicted in Fig. 7. In this case, only the power received from the central pixel, placed at (X = 0, Y = 0) is considered. There is a good agreement between the measured and simulated results for small tilting angles, and in both cases it can be observed how quickly the received power decreases when the plate is no longer pointing to the main reflector center.

B. Example 2: Human body torso

In this second example, a more realistic case is considered. The target of this experiment was a female mannequin placed

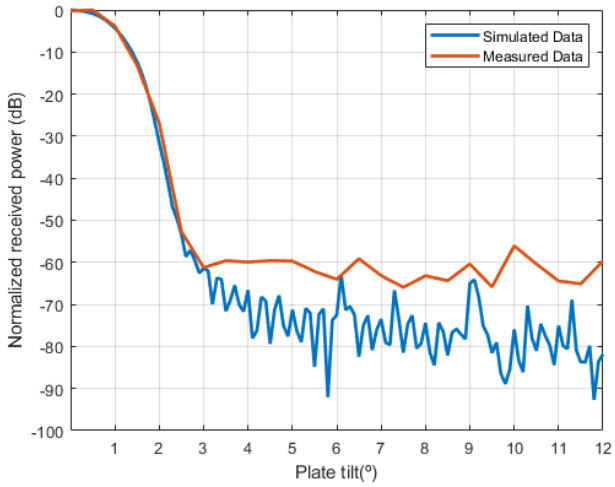

Fig. 7. Normalized power obtained at the receiver as a function of the tilt of the metallic plate for the central pixel placed at (X = 0, Y = 0) for measurements and simulation.

once again at 8 m standoff from the imaging system. This target presents a more complex geometry due to the curvature of the human body. As previously noted (see Section V-A), the response of the system gets much worse when the response of the OUT moves away from the direction of the specular reflection. For this reason, this example is very interesting, because it allows analyzing the performance of the system in more complicated and realistic conditions.

In order to accomplish the simulation of the same target, a 3-D model of the mannequin shown in Fig. 8 was obtained using a consumer infrared structured light depth sensor that is moved around the surface of the mannequin [22]. Fig. 9(a) shows the CAD model imported into the simulator. In Fig. 9(b) the same mesh is coded in range from the antenna in order to compare the obtained range results using both measurements and simulations. The simulations are performed in a 90 cm $\times$ 50 cm observation grid in the target area. According to the results in [17], at these frequencies the plastic material of the mannequin reflects most of the incident electric field which makes the approximation good enough in terms of relative received power and range estimation.

Range images obtained using simulations and measurements are presented in Fig. 10. Range is obtained from the corresponding peak of the IFFT for both the measurement and simulation of each scanned pixel in the target area. Fig. 10(a) presents results for the simulated case while Fig. 10(b) depicts the measured one. The agreement between the measurements and simulations is good, and both results match well the expected range profile of the actual mannequin as depicted in Fig. 9(b).

VI. CONCLUSION

A Physical Optics-based simulator for the analysis of the THz imaging systems based on multireflector configurations has been presented. The simulator is able not only to model the incident field that the focusing system creates on the target

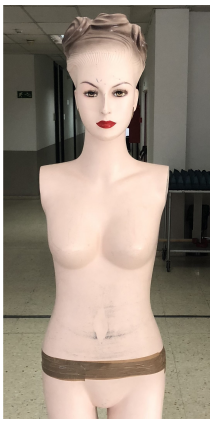

Fig. 8. Picture of the measured female mannequin used to validate the PO simulator.

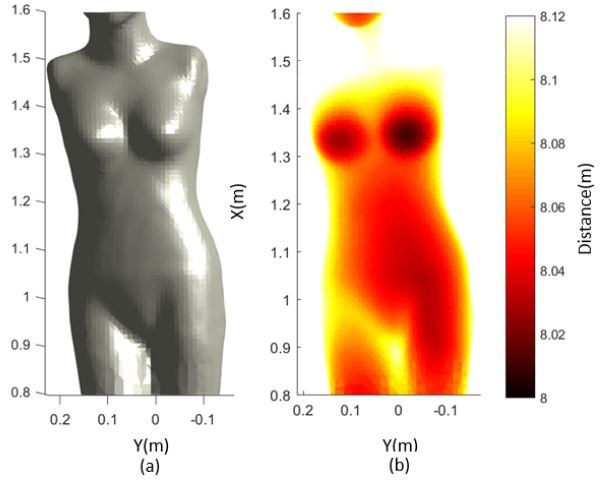

Fig. 9. (a) Imported CAD model of the mannequin; (b) Model coded in depth from the antenna: each pixel represents the distance from the central point of the main reflector to the center of each facet of the model.

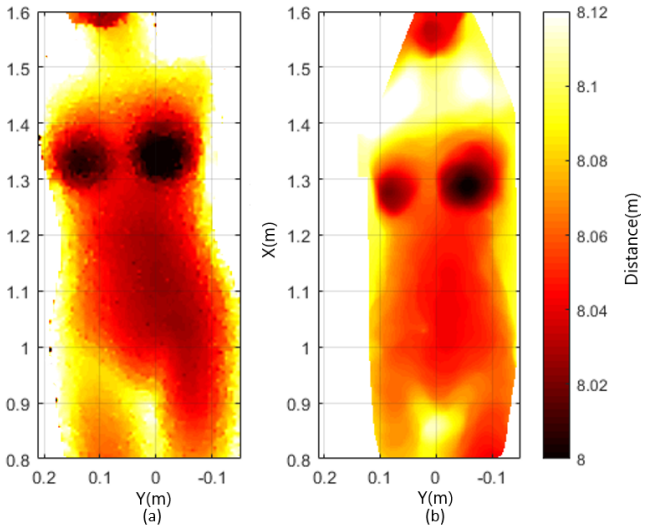

Fig. 10. Depth map (distance from the center of the main reflector to each of the pixels of the imaging plane obtained (a) from simulations and (b) from measurements.

under inspection, but also to calculate the electric field that the target, imported as a CAD model, scatters back to the system receiver. The simulation results have been compared with measurements from an existing real prototype to validate the results of the simulator and good agreement has been obtained. This work is a step forward to improve the design and optimization of novel imaging configurations based on THz radar. Further work will be related with the simulation of targets composed of different materials (e.g. dielectrics).

REFERENCES

[1] S. S. Ahmed, A. Schiessl, F. Gumbmann, M. Tiebout, S. Methfessel, and L. Schmidt, "Advanced microwave imaging," *IEEE Microw. Mag.*, vol. 13, no. 6, pp. 26–43, 2012.

[2] D. Sheen, D. McMakin, and T. Hall, "Three-dimensional millimeter-wave imaging for concealed weapon detection," *IEEE Trans. Microw. Theory Tech.*, vol. 49, no. 9, pp. 1581–1592, 2001.

[3] F. Friederich, W. Von Spiegel, M. Bauer, F. Meng, M. D. Thomson, S. Boppel, A. Lisauskas, B. Hils, V. Krozer, A. Keil *et al.*, "Thz active imaging systems with real-time capabilities," *IEEE Trans. Terahertz Sci. Technol.*, vol. 1, no. 1, pp. 183–200, 2011.

[4] K. Cooper, R. Dengler, N. Llombart, B. Thomas, G. Chattopadhyay, and P. Siegel, "Thz imaging radar for standoff personnel screening," *IEEE Trans. Terahertz Sci. Technol.*, vol. 1, no. 1, pp. 169–182, 2011.

[5] D. M. Sheen, T. E. Hall, R. H. Severtsen, D. L. McMakin, B. K. Hatchell, and P. L. J. Valdez, "Active wideband 350GHz imaging system for concealed-weapon detection," in *Society of Photo-Optical Instrumentation Engineers (SPIE) Conference Series*, ser. Society of Photo-Optical Instrumentation Engineers (SPIE) Conference Series, vol. 7309, May 2009.

[6] C. A. Weg, W. von Spiegel, R. Henneberger, R. Zimmermann, T. Loeffler, and H. G. Roskos, "Fast Active THz Cameras with Ranging Capabilities," *Journal of infrared millimeter and terahertz waves*, vol. 30, no. 12, pp. 1281–1296, DEC 2009, 33rd International Conference on Infrared, Millimeter, and Terahertz Waves, Pasadena, CA, SEP, 2008.

[7] D. A. Robertson, D. G. Macfarlane, R. I. Hunter, S. L. Cassidy, N. Llombart, E. Gandini, T. Bryllert, M. Ferndahl, H. Lindström, J. Tenhunen, H. Vasama, J. Huopana, T. Selkälä, and A. Vuotikka, "A high frame rate, 340 ghz 3d imaging radar for security," in *2018 IEEE Radar Conference (RadarConf18)*, April 2018, pp. 0055–0060.

[8] A. Garcia-Pino, B. Gonzalez-Valdes, O. Rubiños, J. Grajal, A. Badolato, B. Mencia-Oliva, P. G. Soidán, and J. L. Besada-Sanmartín, "Bifocal reflector antenna for a standoff radar imaging system with enhanced field of view," *IEEE Trans. Antennas Propag.*, vol. 62, no. 10, pp. 4997–5006, Oct 2014.

[9] N. Llombart, K. B. Cooper, R. J. Dengler, T. Bryllert, and P. H. Siegel, "Confocal ellipsoidal reflector system for a mechanically scanned active terahertz imager," *IEEE Trans. Antennas Propag.*, vol. PP, no. 99, pp. 1 –1, 2010.

[10] A. Garcia-Pino, N. Llombart, B. Gonzalez-Valdes, and O. Rubinos-Lopez, "A bifocal ellipsoidal gregorian reflector system for THz imaging applications," *IEEE Trans. Antennas Propag.*, vol. 60, no. 9, pp. 4119–4129, 2012.

[11] M. R. Hajihashemi and M. El-Shenawee, "Shape reconstruction using the level set method for microwave applications," *IEEE Antennas and Wireless Propagation Letters*, vol. 7, pp. 92–96, 2008.

[12] G. Ortiz-Jiménez, F. García-Rial, L. A. Úbeda Medina, R. Pagés, N. García, and J. Grajal, "Simulation framework for a 3-d high-resolution imaging radar at 300 ghz with a scattering model based on rendering techniques," *IEEE Trans. Terahertz Sci. Technol.*, vol. 7, no. 4, pp. 404–414, July 2017.

[13] P. Beckmann and A. Spizzichino, "The scattering of electromagnetic waves from rough surfaces," *Norwood, MA, Artech House, Inc., 1987, 511 p.*, 1987.

[14] U. S. N. B. of Standards and F. E. Nicodemus, *Geometrical considerations and nomenclature for reflectance*. US Department of Commerce, National Bureau of Standards, 1977, vol. 160.

[15] J. A. Martinez-Lorenzo, A. G. Pino, I. Vega, M. Arias, and O. Rubinos, "Icara: Induced-current analysis of reflector antennas," *IEEE Antennas Propag. Mag.*, vol. 47, no. 2, pp. 92–100, 2005.

[16] L. E. Tirado, J. A. Martinez-Lorenzo, B. Gonzalez-Valdes, C. Rappaport, O. Rubinos-Lopez, and H. Gomez-Sousa, "GPU implementation of the modified equivalent current approximation (MECA) method," *Applied computational electromagnetics society journal*, no. 9, SEP 2012.
[17] J. Grajal, A. Badolato, G. Rubio-Cidre, L. Úbeda Medina, B. Mencia-Oliva, A. Garcia-Pino, B. Gonzalez-Valdes, and O. Rubiños, "3-d high-resolution imaging radar at 300 ghz with enhanced fov," *IEEE Trans. Microw. Theory Tech.*, vol. 63, no. 3, pp. 1097–1107, March 2015.
[18] A. M. Arias, J. O. Rubiños, I. Cuiñas, and A. G. Pino, "Electromagnetic scattering of reflector antennas by fast physical optics algorithms," *Recent Res. Devel. Magnetics*, vol. 1, no. 1, pp. 43–63, 2000.
[19] M. Arias-Acuña, A. García-Pino, and O. Rubiños-López, "Fast far field computation of single and dual reflector antennas," *Journal of Engineering*, vol. 2013, 2013.
[20] H. Gómez Sousa, J. Á. Martínez Lorenzo, Ó. Rubiños López, J. Gutiérrez Meana, M. Graña Varela, B. González Valdés, and M. Arias Acuña, "Strategies for improving the use of the memory hierarchy in an implementation of the modified equivalent current approximation (meca) method," *Applied Computational Electromagnetics Society Journal*, 2010.
[21] D. R. Wehner, *High-resolution Radar*, 2nd ed. Artech House, 1995.
[22] R. A. Newcombe, S. Izadi, O. Hilliges, D. Molyneaux, D. Kim, A. J. Davison, P. Kohi, J. Shotton, S. Hodges, and A. Fitzgibbon, "Kinectfusion: Real-time dense surface mapping and tracking," in *Mixed and augmented reality (ISMAR), 2011 10th IEEE international symposium on*. IEEE, 2011, pp. 127–136.

Lorena Perez-Eijo received the B. Sc. and M. Sc. degree in Electrical Engineering from the University of Vigo, Vigo, Spain, in 2014. She is with the Antenna and Optical Communications Group at the University of Vigo since 2014 and she is currently working towards her Ph. D. degree. Her research interests include radar signal processing, RCS measurements, inverse scattering, advanced imaging techniques and THz technology for electromagnetic sensing applications.

Borja Gonzalez-Valdes (S'07M'10) received the B.S. and Ph.D. degrees in electrical engineering from the University of Vigo, Vigo, Spain, in 2006 and 2010, respectively. From 2006 to 2010, he was with the Antenna and Optical Communications Group at the University of Vigo. During 2008 and 2009, he was a Visiting Researcher at the Gordon CenSSIS, Northeastern University. In 2011, he joined the ALERT Center of Excellence, Northeastern University. In 2015 he joined the Signal and Communications Theory department at University of Vigo as a postdoctoral researcher, where he became a Ramon y Cajal fellow in 2018 the University of Vigo. Since 2019 he is an Associate Professor at the University of Vigo. His research interests include antenna design, inverse scattering, radar, advanced imaging techniques, Unmaned Aerial Vehicles and THz technology. He has authored or coauthored more than 100 publications, including over 35 journal papers.

Marcos Arias Acuña was born in Vigo, Spain on June 1, 1968. He got the Telecommunications Engineer degree and the PhD in Telecommunication Engineering from the University of Vigo in 1991 and 1997 respectively. He is Associate Professor since 1998 and has been with the Department of Signal Theory and Communications teaching radiocommunications since 1992. He has worked in projects related with antennas for satellite and radioastronomy, communication systems such DVB-T, LMDS and UMTS and system engineering.

Dario Tilves received the Bachelor's and Master's degrees in telecommunication engineering from the University of Vigo, Vigo, Spain, in 2016 and 2018, respectively. From 2016 to 2018, he was with the Antenna, Radar and Optical Communications Group at the University of Vigo. From 2018 to 2019, he was with the Multimedia Technology Group at the University of Vigo. His research interests include physical optics, sign language recognition, artificial neural network and deep learning.

Yolanda Rodriguez-Vaqueiro is a Postdoctoral Researcher affiliated with AtlantTIC Research Center, University of Vigo, (Spain). Yolanda obtained B.S. and M.S. degrees in Electrical Engineering from University of Vigo (Spain) in December 2009, where she was also granted as Junior Researcher. In 2011 she obtained a Research Assistant grant from the ALERT (Awareness and Localization of Explosive Related Threats) Center of Excellence at Northeastern University (Boston, MA, USA). In May 2015 she completed her Ph.D. in Electrical Engineering from Northeastern University, after defending her thesis: "Compressive Sensing for Electromagnetic Imaging Using a Nesterov-Based Algorithm". Her work during the Ph.D. studies was recognized with the "Research-Impact Award" by the Electrical and Computer Engineering Department of Northeastern University. Last year she was awarded with a "Juan de la Cierva" grant by the Spanish Ministry of Education. During the course of her career she obtained several awards: "Best Paper award" in the 2012 IEEE Homeland Security Conference, "Honorable Mention in the Student Paper Competition" in the 2013 IEEE APS/URSI Conference, "Best Paper Award" in the 2014 European Conference on Antennas and Propagation, and "Burke/Yannas Award" to the most original research study in the field of bioengineering in the 2015 American Burn Association (ABA) Meeting.

Oscar Rubiños-López was born in Ourense (Spain) in 1968. He received the M.Sc. and Ph.D. degrees in telecommunications engineering from the Universidad de Vigo, Spain, in 1991 and 1997, respectively. Since 2012 he has been a Full Professor in the Department of Signal Theory and Communications, Universidad de Vigo. During different periods in 2004, 2005, and 2007, he was a Visiting Researcher with the Chalmers University of Technology, Göteborg, Sweden. From 2001 to 2006, he was the Vice President of the University Extension (2001–2002) and for University Extension and Students at the Universidad de Vigo (2002-2006). He is currently commissioned of new projects at University of Vigo. He has coauthored more than 100 technical journal and conference papers. His research interests include the analysis and design of broadband antennas, numerical simulation of applied electromagnetic problems, terahertz technology for electromagnetic sensing applications, satellite systems and wireless communications.

Antonio Pino (S'87-M'89) was born in Valdemoro, Madrid, Spain, in 1962. He received the M.S. degree in 1985 and the Ph.D. degree in 1989, both in telecommunications engineering from the Polytechnic University of Madrid (UPM). From 1985 to 1989 he was with the Radiation Group of UPM as a Research Assistant. He joined the Department of Technologies of Communications at University of Vigo (Spain) as Associate Professor in 1989, becoming full Professor in 1994. During 1993 he was a Visiting Researcher at the Center for Electromagnetics Research, Northeastern University, Boston. His research interests include reflectarray and shaped reflector antennas for communication and radar applications, high frequency backscattering, computational electromagnetics, and THz technology. In these topics he is author of more than 100 technical papers in journal and conferences and he has been advisor of 14 Ph.D. Thesis. He became senior member of IEEE in 2005. From 2006 to 2010 he was Vice-Rector of Academic Organization and Faculty, and since 2014 he is the Director of the International Doctoral School, both at University of Vigo.

Federico García-Rial (GS'18) was born in Pensacola, USA, in 1991. He received his B. Sc. and M. Sc. degree in Electrical Engineering from the Technical University of Madrid (UPM), Spain, in 2015, and is currently working towards his Ph. D. degree. Since 2014, he has been with the Microwave and Radar Group, of the Department of Signals, Systems and Radiocommunications at the Technical University of Madrid. His research interests are in the area of radar signal processing, THz imaging, and electronic countermeasures.

Jesús Grajal (M'17) was born in Toral de los Guzmanes, Leon, Spain, in 1967. He received his Ingeniero de Telecomunicacion degree and the PhD degree from the Universidad Politécnica de Madrid (UPM), Spain, in 1992 and 1998, respectively. Since 2017 he has been a full professor at the Signals, Systems, and Radiocommunications Department of the Universidad Politécnica de Madrid. His current research interests include hardware design for radar systems, radar signal processing, and broadband digital receivers for radar and spectrum surveillance applications.